RSC Advances

PAPER

View Article Online
View Journal | View Issue

Cite this: *RSC Adv.*, 2024, **14**, 13445

NMR analysis of structural geometry and molecular dynamics in perovskite-type $N(CH_3)_4CdBr_3$ crystal near high-temperature phase transition

Ae Ran Lim *[ab] and Sun Ha Kim[cd]

Received 23rd March 2024
Accepted 15th April 2024

DOI: 10.1039/d4ra02220c

rsc.li/rsc-advances

The NMR chemical shifts, linewidths, spin–lattice relaxation times in the rotating system $T_{1\rho}$, and spin–lattice relaxation times in the laboratory system T_1 were evaluated for the perovskite-type $N(CH_3)_4CdBr_3$ crystal, aiming to understand the changes in the structural geometry and molecular dynamics from phase I to phase II. From the temperature-dependence of the ^{1}H, ^{13}C, ^{14}N, and ^{113}Cd NMR chemical shifts, the structural geometry underwent a continuous change, without anomalous changes around (T_C = 390 K). However, the linewidths in phase I were narrower than those in phase II, indicating that the motional averaging effects were caused by the rapid rotation of the $N(CH_3)_4$ group. Sudden changes in T_1 and $T_{1\rho}$ were observed near T_C, for which the activation energy E_a in phase I was approximately 12 times larger than that in phase II; the small E_a values in phase II indicate a large degree of freedom for the methyl group and $CdBr_6$ octahedra, whereas the large E_a in phase I was primarily attributed to the overall $N(CH_3)_4$ and the ^{113}Cd in the $CdBr_6$ groups. Consequently, the phase transition mechanisms of $N(CH_3)_4CdBr_3$ are related to reorientation of the $N(CH_3)_4$ group and the arrangement of the $CdBr_6$ groups.

1. Introduction

ABX_3 perovskites are an interesting group of compounds that undergo phase transition accompanied by remarkable changes in their physical and chemical properties.[1–7] Many studies on organic–inorganic hybrid compounds have yielded meaningful results because of the wide applicability of these materials.[8–17] Tetramethylammonium tribromocadmate ($N(CH_3)_4CdBr_3$) belongs to the $N(CH_3)_4BX_3$ (B = ^{55}Mn, ^{59}Co, ^{64}Cu, ^{65}Zn, ^{113}Cd; X = ^{35}Cl or ^{79}Br) family of ABX_3-type perovskites.[18–29] The crystal structure at room temperature consists of isolated linear chains of face-sharing $CdBr_6$ octahedra separated by $N(CH_3)_4$ ions. $N(CH_3)_4CdBr_3$ has two phase transition temperatures, 160 and 390 K,[19,22,23] with three phases denoted as III, II, and I, respectively, in the order of increasing temperature. The high-temperature transition is a second-order process, whereas the low-temperature transition is a weak first-order phase transition. In phase I (above 390 K), $N(CH_3)_4CdBr_3$ adopts a hexagonal structure in the space group $P6_3/mmc$ with Z = 2. In phase II (below 390 K), the crystal exhibits the same hexagonal structure in space group $P6_3/m$ with Z = 2. At room temperature, the crystal structure is hexagonal with lattice constants of $a = b$ = 9.404 Å, c = 6.990 Å, $\alpha = \beta$ = 90°, and γ = 120°.[20] The phase transition at 160 K leads to another hexagonal phase with space group $P6_1$ and Z = 6. The cell dimensions in phase III are characterized by the lattice constants $a = b$ = 9.257 Å, c = 20.900 Å, $\alpha = \beta$ = 90°, and γ = 120°,[24,26] where the c-axis is three times longer compared to that in phase II. The structures, space groups, lattice constants, and Z in the phases I, II, III are summarized in Table 1.

In a previous study, the ^{1}H nuclear magnetic resonance (NMR) spin–lattice relaxation time T_1 in the laboratory frame did not reveal any anomaly in the temperature range of 77–400 K for $N(CH_3)_4CdBr_3$.[18] This phenomenon can be explained by the relaxation mechanism owing to the fast reorientation of the CH_3 groups. According to a previous report by Baisa *et al.*,[25] a singlet ^{79}Br nuclear quadrupole resonance (NQR) spectrum was obtained for phases II and I, and a triplet spectrum was recorded for phase III. In addition, the NMR T_1 for ^{79}Br near 160

Table 1 Structures, space groups, lattice constants (Å), and Z at phases I, II, and III for $N(CH_3)_4CdBr_3$

Phase	III	II	I
Structure	Hexagonal	Hexagonal	Hexagonal
Space group	$P6_1$	$P6_3/m$	$P6_3/mmc$
Lattice constants	$a = b$ = 9.257 c = 20.900 $\alpha = \beta$ = 90° γ = 120°	$a = b$ = 9.404 c = 6.990 $\alpha = \beta$ = 90° γ = 120°	
Z	6	2	2
Reference	24 and 26	20	20

[a]Graduate School of Carbon Convergence Engineering, Jeonju University, Jeonju 55069, Korea
[b]Department of Science Education, Jeonju University, Jeonju 55069, Korea. E-mail: aeranlim@hanmail.net; arlim@jj.ac.kr
[c]Korea Basic Science Institute, Seoul Western Center, Seoul 03759, Korea
[d]Department of Chemistry, Kyungpook National University, Daegu 41566, Korea

K exhibits strong temperature dependence and changes by three orders of magnitude in the temperature range of 77–310 K.[27] Overall, the relaxation processes of ^{1}H and ^{79}Br in $N(CH_3)_4CdBr_3$ near the phase-transition temperature of 160 K were studied in the laboratory frame using static NMR. The structural phase transition near the high phase-transition temperature of 390 K presented by our group in the past was briefly studied using magic angle spinning (MAS) NMR in the rotating frame and static NMR in the laboratory frame.[30]

Measurements of the spin–lattice relaxation time in the rotating system ($T_{1\rho}$) have the advantage of probing the molecular motion within the kHz range, whereas the spin–lattice relaxation time in the laboratory system (T_1) reflects motion within the MHz range.

Although various experimental results have been reported for $N(CH_3)_4CdBr_3$, the structural geometry and the molecular motion associated with the phase transitions remain undisclosed. This study is expected to provide important insights into the characteristics regarding the advancements in perovskite materials. Therefore, $N(CH_3)_4CdBr_3$ single crystals are grown, and it was confirmed that the high phase-transition temperature occurs at (T_C =390 K). The crystal structure is also confirmed to be hexagonal, using single-crystal X-ray diffraction (SCXRD) experiments. The temperature dependence of the ^{1}H and ^{13}C MAS NMR chemical shifts is obtained to elucidate the changes in the structural geometry related to the phase transition. The temperature dependences of the ^{14}N and ^{113}Cd NMR chemical shifts near T_C in the laboratory system are also measured. In addition, the spin–lattice relaxation times in the rotating system ($T_{1\rho}$) for ^{1}H and ^{13}C as a function of temperature are considered, and the corresponding spin–lattice relaxation times in the laboratory system (T_1) for ^{113}Cd are measured by a static NMR method. Based on these results, the activation energies near the phase-transition temperature of 390 K are discussed in relation to the role of the $N(CH_3)_4$ group in the cation and Cd in the anion.

2. Experimental

2.1. Crystal growth

Single crystals of $N(CH_3)_4CdBr_3$ were grown by slow evaporation method using $N(CH_3)_4Br$ (Aldrich, 98%) and $CdBr_2$ (Aldrich, 98%) in a molecular weight ratio of 2 : 1, in an aqueous solution. However, $N(CH_3)_4CdBr_3$ crystals did not grow well at a ratio of 1 : 1 molar composition. $N(CH_3)_4Br$ and $CdBr_2$ compounds with the ratio of 2 : 1 were dissolved in distilled water, and stirred and heated at a slightly higher temperature to obtain a completely saturated solution. The single crystals obtained by slow evaporation after a few weeks in a thermostat at 300 K were hexagonal in shape, transparent and colorless with dimensions of $7 \times 3 \times 2$ mm^3. To prevent degradation from moisture in the air, the crystals were stored in a desiccator.

2.2. Characterization

Differential scanning calorimetry (DSC) curves were obtained using a DSC instrument at a heating and cooling rate of 10 °C min^{-1} in the 200–570 K range under a flow of dry nitrogen gas. The variation in the crystal morphology with respect to the temperature change was observed using an optical polarizing microscope (Carl Zeiss) on a hot stage (Linkam THMS 600).

The structure and lattice parameters at 250 and 300 K were determined using single-crystal X-ray diffraction (SCXRD) at the Korea Basic Science Institute (KBSI) of the Seoul Western Centre. The crystal was mounted on a diffractometer (Bruker D8 Venture PHOTON III M14) with a graphite-monochromated Mo Kα target and a nitrogen cold stream (−50 °C). Data were collected using the SMART APEX3 and SAINT programs and absorption-corrected using the multiscan method in SADABS. The single-crystal structure was analyzed using direct methods and supplemented with least squares analysis of the entire F^2 matrix using SHELXTL.[31] All non-hydrogen atoms were anisotropically refined, and the hydrogen atoms were included at geometrically ideal positions. Further, the powder X-ray diffraction (PXRD) patterns were obtained at 300 K and 410 K using an XRD spectrometer with a Mo Kα radiation source by utilizing the SCXRD method.[32]

NMR spectra of the $N(CH_3)_4CdBr_3$ crystals were recorded using a solid-state NMR spectrometer (Bruker 400 MHz Avance II+) at KBSI. The ^{1}H magic angle spinning (MAS) NMR data at the Larmor frequency of $\omega_o/2\pi = 400.13$ MHz and the ^{13}C MAS NMR data at the Larmor frequency of $\omega_o/2\pi = 100.61$ MHz were measured as a function of temperature. To minimize the spinning sideband, the MAS speed was measured at 10 kHz. ^{1}H and ^{13}C chemical shifts were recorded using tetramethylsilane as the standard. The one-dimensional (1D) NMR spectra of ^{1}H and ^{13}C were obtained with a delay time of 0.5 s. The ^{1}H and ^{13}C spin–lattice relaxation times in the rotating system ($T_{1\rho}$) were measured with delay times from 200 μs to 100 ms; a 90° pulse was used for acquiring ^{1}H and ^{13}C data, with a delay of 3.6–3.8 μs. In addition, the static ^{14}N NMR chemical shift at a Larmor frequency $\omega_o/2\pi = 28.90$ MHz was monitored with increasing temperature. The ^{14}N NMR chemical shift was determined using NH_4NO_3 as the reference standard, and ^{14}N NMR spectra were obtained using a solid-state echo sequence. The static NMR spectra for the ^{113}Cd nucleus at $\omega_o/2\pi = 88.73$ MHz were obtained using the same NMR spectrometer. The spin–lattice relaxation time in the laboratory system (T_1) was measured by applying the pulse sequence method. A 90° pulse width was used for ^{113}Cd at 4.3 μs. Temperature-dependent NMR spectra were obtained between 180 and 430 K. The temperature was maintained by controlling the N_2 gas flow and heater current within an accuracy of ±0.5 K.

3. Results and discussion

3.1. Single-crystal XRD

SCXRD analysis at 250 and 300 K revealed that $N(CH_3)_4CdBr_3$ crystallized with a hexagonal structure belonging to space group $P6_3/m$. At 250 K, the lattice parameters are $a = b = 9.3878$ (4) Å, $c = 6.9957$ (5) Å, $\alpha = \beta = 90°$, $\gamma = 120°$, and $Z = 2$, whereas the lattice constants at 300 K are $a = b = 9.417$ (3) Å, $c = 7.0002$ (3) Å, $\alpha = \beta = 90°$, $\gamma = 120°$, and $Z = 2$. The crystal structure is composed of isolated linear chains of face-shared $CdBr_6$

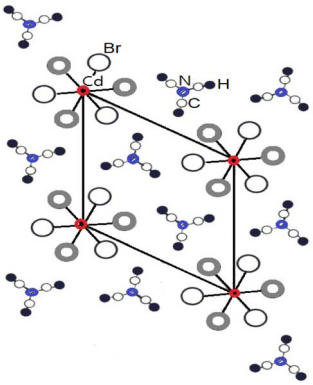

Fig. 1 Projection of the unit cell of hexagonal $N(CH_3)_4CdBr_3$ at room temperature along the *c*-axis (big open circle Br in the $+z$ and gray circle Br in $-z$).

octahedra, which are widely separated by $N(CH_3)_4$ ions. Here, the bond lengths for C–H are approximately 0.91 Å.[26] The single-crystal structure with the chains of $CdBr_6$ octahedra parallel to the *c*-axis are shown in Fig. 1.[20] Cd^{2+} is at the origin and three Br^- ions form a regular triangle. Br on the $+z$ axis is shown as open circles, and Br on the $-z$ axis is shown as gray circles.

3.2. Phase-transition temperature

DSC analysis of the $N(CH_3)_4CdBr_3$ crystals was performed at a heating and cooling rate of 10 °C min^{-1} with a sample amount of 15.70 mg. The DSC curves show weak endothermic and exothermic peaks near 390 K during heating and cooling, respectively (Fig. 2(a)); the corresponding enthalpy for the peak was 300 J mol^{-1}. The endothermic peak at 390 K corresponds to the phase-transition temperature, arising from the transition from one hexagonal structure to another. The phase transition at this temperature was reversible. Variable-temperature optical polarizing microscopy analysis of the morphology shows that the single crystals did not change until the temperature was increased from 300 to 573 K. The morphologies of the $N(CH_3)_4CdBr_3$ single crystal at (a) 300 K, (b) 350 K, (c) 430 K, and (d) 300 K (after cooling) are shown in the inset of Fig. 2(b).

PXRD analysis was performed below and above the phase-transition temperature, in the 2θ range of 8–60° (Fig. 2(b)). The PXRD pattern recorded at 300 K (blue) differs slightly from that recorded at 410 K (violet). This result correlates well with the endothermic peak obtained from the DSC results; this difference is related to the phase transition temperature, T_C (=390 K). The PXRD pattern (dark yellow) obtained after cooling from 410 to 300 K matches well with the results obtained at 300 K before heating. The DSC and PXRD results show that the phase transition is reversible.

3.3. NMR chemical shifts and linewidths for ^1H and ^{13}C

Structural analysis was performed by monitoring ^1H in $N(CH_3)_4CdBr_3$ using MAS NMR at increasing temperatures. The temperature-dependences of the ^1H NMR chemical shifts and linewidths are shown in Fig. 3. At 300 K, the ^1H NMR chemical

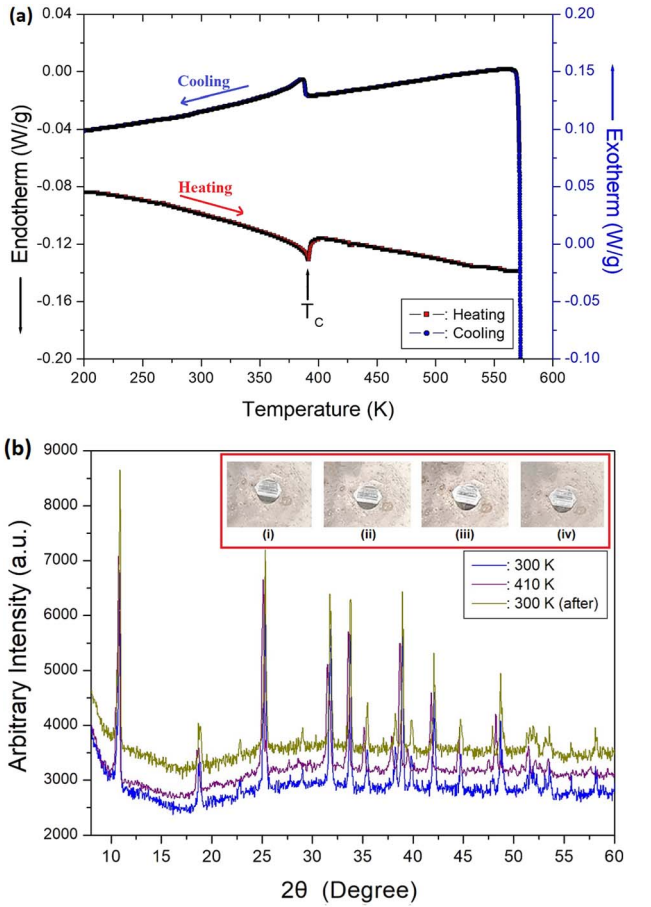

Fig. 2 (a). Differential scanning calorimetry curves at heating and cooling rate of 10 °C min^{-1}. (b). The powder X-ray diffraction patterns at 300, 410, and 300 K (after) ((Inset): the morphologies at (i) 300 K, (ii) 350 K, (iii) 430 K, and (iv) 300 K (after cooling) of $N(CH_3)_4CdBr_3$ single crystal).

shift appearing at approximately $\delta = 3.57$ ppm (inset of Fig. 3) is assigned to the methyl proton. The sidebands for the proton signal obtained at a spinning speed of 10 kHz are indicated by open circles. The ^1H NMR chemical shifts were nearly continuous within the error range, without any anomalous changes near T_C as the temperature increased. The full-width-at-half-maximum (FWHM) in the ^1H NMR spectrum increased as the temperature increased and then decreased again rapidly near T_C; the FWHM decreased from 2 ppm at 300 K to 1.67 ppm near T_C.

The temperature-dependences of the NMR chemical shifts and ^{13}C linewidths for $N(CH_3)_4CdBr_3$ are shown in Fig. 4. The ^{13}C MAS NMR spectrum at 300 K exhibited one resonance signal (inset of Fig. 4) and a ^{13}C chemical shift was recorded at 58.82 ppm, related to the methyl carbon. With increasing temperature, the ^{13}C NMR chemical shift moved from 58.09 to 59.49 ppm without an anomalous change near T_C, but increased almost linearly with increasing temperature. The continuous change in the NMR chemical shifts due to the local field around the ^{13}C nuclei indicates changes in the crystallographic geometry, without anomalous changes near T_C. The ^{13}C linewidth decreased from 0.35 ppm at 300 K to 0.26 ppm near T_C, similar

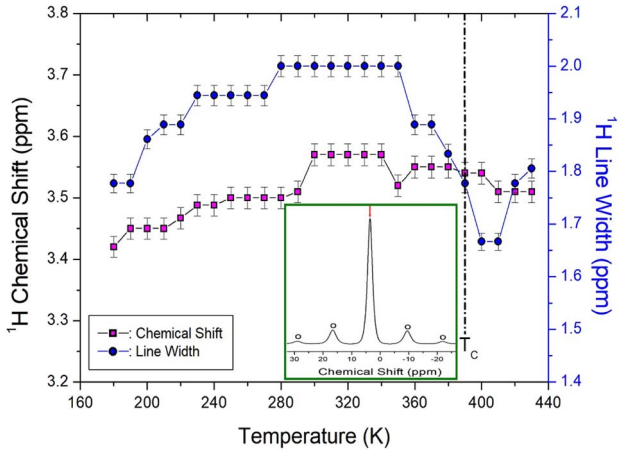

Fig. 3 NMR chemical shifts and line widths for ^{1}H in $N(CH_3)_4CdBr_3$ as the temperature rises ((Inset): The ^{1}H NMR spectrum at 300 K, and open circles are spinning sidebands).

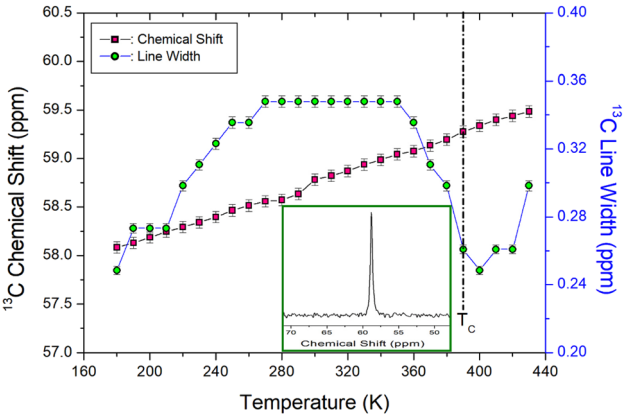

Fig. 4 NMR chemical shifts and line widths for ^{13}C in $N(CH_3)_4CdBr_3$ as the temperature rises ((Inset): The ^{13}C NMR spectrum at 300 K).

to the change in the linewidth of ^{1}H. This implies that the sources of the interactions between the atoms and ions around the ^{1}H and ^{13}C nuclei are similar. The ^{13}C linewidths were very small compared to the ^{1}H linewidths. The less broadening of the linewidths for ^{1}H and ^{13}C near 160 K are thought to be due to the low phase-transition temperature.

3.4. ^{1}H and ^{13}C NMR spin–lattice relaxation times in the rotating system, $T_{1\rho}$

The changes in the intensity of the ^{1}H and ^{13}C NMR signals with variation of the delay times were recorded at a given temperature, and the relationship to the decay rate of the magnetization was defined by the spin–lattice relaxation time, $T_{1\rho}$:[33,34]

$$P(\tau)/P(0) = A\exp(-\tau/T_{1\rho}) \quad (1)$$

where $P(\tau)$ is the signal intensity at time τ and $P(0)$ is the signal intensity at time $\tau = 0$. The ^{1}H $T_{1\rho}$ and ^{13}C $T_{1\rho}$ values for $N(CH_3)_4CdBr_3$ were obtained from the slope of the intensity *vs.* delay time plot using eqn (1). As shown in Fig. 5, the ^{1}H $T_{1\rho}$ and

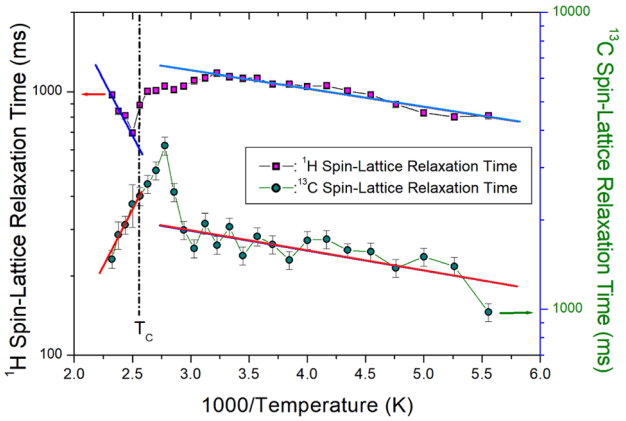

Fig. 5 The spin–lattice relaxation times in the rotating system $T_{1\rho}$ for ^{1}H and ^{13}C in $N(CH_3)_4CdBr_3$ as a function of inverse temperature. The slopes of the solid lines are represented activation energies.

^{13}C $T_{1\rho}$ values were of the order of milliseconds, and the ^{1}H and ^{13}C $T_{1\rho}$ values slowly increased below T_C. In contrast, above T_C, the ^{13}C $T_{1\rho}$ values, unlike ^{1}H $T_{1\rho}$, decreased rapidly. This trend at high temperature is not general, but the activation energy mentioned below is almost the same. Although the distinct proton and carbon dynamics at high temperature are not yet understood, we attribute this result to the disparity between the ^{13}C NMR frequency of 100.61 MHz and the ^{1}H NMR frequency of 400.13 MHz. Furthermore, above T_C, the molecular motions of ^{1}H become more constrained, whereas those of ^{13}C remain relatively unrestricted. The Arrhenius plots for the $T_{1\rho}$ molecular motions with the relaxation time are separated into fast- and slow-motion regions. The fast motion is represented as $\omega_1\tau_C \ll 1$, $T_{1\rho}{}^{-1} \propto \exp(E_a/k_BT)$ and the slow motion as $\omega_1\tau_C \gg 1$, $T_{1\rho}{}^{-1} \propto \omega_1{}^{-2}\exp(-E_a/k_BT)$.[34] The plot is separated into different motion areas at a temperature that is approximately 50 K lower than the phase transition temperature. At low temperatures, the ^{1}H $T_{1\rho}$ and ^{13}C $T_{1\rho}$ values were in the fast-motion region. At high temperatures, the ^{13}C $T_{1\rho}$ values were attributed to the slow-motion region, whereas the ^{1}H $T_{1\rho}$ values were related to the fast-motion region.

Based on Bloembergen–Purcell–Pound (BPP) theory, the experimental values of $T_{1\rho}$ can be expressed by the correlation time τ_C for re-orientational motion, and $T_{1\rho}$ for molecular motion as follows:[35–37]

$$\begin{aligned} 1/T_{1\rho} = R\{&4\tau_C/[1+\omega_1{}^2\tau_C{}^2] + \tau_C/[1+(\omega_C-\omega_H)^2\tau_C{}^2] \\ &+ 3\tau_C/[1+\omega_C{}^2\tau_C{}^2] + 6\tau_C/[1+(\omega_C+\omega_H)^2\tau_C{}^2] \\ &+ 6\tau_C/[1+\omega_H{}^2\tau_C{}^2]\} = A\exp(-E_a/k_BT) \end{aligned} \quad (2)$$

where R is a constant, ω_1 is the spin-locking field, and ω_C and ω_H are the Larmor frequency of ^{13}C and ^{1}H, respectively. Local field fluctuations are caused by thermal motion, which is activated by thermal energy. The ^{1}H and ^{13}C $T_{1\rho}$ values exhibited similar variations due to similar molecular motions of the C–H bond. $T_{1\rho}$ is generally expressed by an Arrhenius-type equation based on the activation energy (E_a) for molecular motion and temperature. The E_a for ^{1}H obtained from the slope of the $T_{1\rho}$ *vs.*

1000/temperature plot (represented by red squares in Fig. 5) at low and high temperatures was 1.23 ± 0.10 and 14.87 ± 2.25 kJ mol^{-1}, respectively. We compared the values of E_a for CH_3 and $N(CH_3)_4$ motion with those reported for similar systems previously.[38–42] E_a values for methyl group rotation were much smaller than E_a for $N(CH_3)_4$ motions in $N(CH_3)_4$-based compounds. Small E_a values have been reported in other compounds as well; for example, approximately 7.31 kJ mol^{-1} for D-amphetamine sulfate,[43] about 5 kJ mol^{-1} for 2 *t*-butyldimethylsilyloxy-6-bromo-naphthalene,[44] and 3.8 kJ mol^{-1} for $[N(CH_3)_4]_2SeBr_6$.[45] E_a values for $N(CH_3)_4$ motion, however, are much larger, ranging from 18 kJ mol^{-1} to 54 kJ mol^{-1} for $N(CH_3)_4$ halides. Therefore, $N(CH_3)_4CdBr_3$ seems to undergo methyl and $N(CH_3)_4$ motions below and above T_C, respectively.

In addition, the E_a for ^{13}C obtained from the slope of $T_{1\rho}$ *vs.* 1000/temperature (represented by green circles in Fig. 5) at low and high temperatures was 1.14 ± 0.25 and 16.17 ± 1.83 kJ mol^{-1}, respectively. Here, E_a is determined at temperatures ranging from 180 to 340 K below T_C and from 390 to 430 K above T_C.

To determine the sample temperature by spinning rate during MAS NMR experiments, the variance between the set temperature and the actual sample temperature inside the probe was previously reported by Guan and Stark. The equation for the fast MAS probe is cited as[46,47]

$$T_s\,(f) = 0.98\ T_o + 3.79\ (^\circ\mathrm{C})\exp(\omega_s/19.6\ \mathrm{kHz}) - 3.49\ (^\circ\mathrm{C}) \quad (3)$$

where T_o is the set temperature and ω_s is the MAS spinning rate. For example, a set temperature of 360 K for a sample spinning rate of 10 kHz corresponds to 361 K in the fast MAS probe. The temperature variation indicated by DSC and NMR is minimal for the fast MAS probe.

3.5. Static ^{14}N NMR chemical shifts and linewidths

The ^{14}N static NMR spectra of the $N(CH_3)_4CdBr_3$ single crystal were obtained with variation of the temperature in the range of 180–420 K using the solid-state echo method. An external magnetic field of 9.4 T was applied to the single crystal in an arbitrary axial direction. The ^{14}N NMR chemical shifts spanned a significantly wider range than the ^1H and ^{13}C chemical shifts, suggesting that valuable insight can be gained by considering the surrounding environment of ^{14}N. Because the spin number of ^{14}N is $I = 1$, the NMR spectrum is expected to have two resonance lines owing to quadrupole interactions.[33] Two ^{14}N NMR signals appeared on the left and right sides of the zero point of the chemical shifts with variation of the temperature, as shown in Fig. 6(a). At 300 K, ^{14}N NMR signals were recorded at 16.69 and 12.80 ppm. As the temperature increased, the ^{14}N NMR chemical shifts decreased slightly without any change near T_C (Fig. 6(b)); the surrounding environment of ^{14}N hardly changes as the temperature increases. The reduction in ^{14}N NMR signal intensity with increasing temperature is caused by cross-linking with ^{13}C around the ^{14}N nuclei. The ^{14}N linewidth was broad as approximately 17.30 ppm at low temperatures, and the linewidth as the temperature increased became slightly narrower. As the temperature increased, it was found that

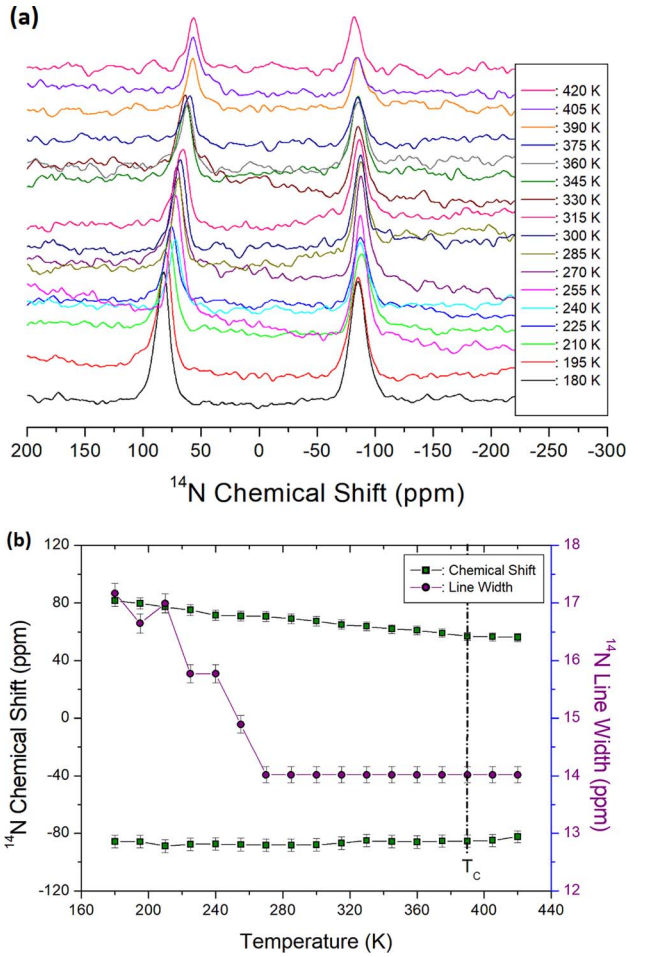

Fig. 6 (a). Static NMR spectrum for ^{14}N in $N(CH_3)_4CdBr_3$ single crystal as the temperature rises. (b). Static NMR chemical shifts and line widths for ^{14}N in $N(CH_3)_4CdBr_3$ single crystal as the temperature rises.

although there was little change in the ^{14}N NMR chemical shift, molecular motion due to line width became very active.

3.6. Static ^{113}Cd NMR chemical shifts and spin–lattice relaxation times in the laboratory system, T_1

The natural abundance and spin number of ^{113}Cd are 12.3% and $I = 1/2$, respectively;[33,37] the peak has relatively high NMR sensitivity. Therefore, ^{113}Cd NMR spectroscopy is used to examine the structural geometries and molecular dynamics of various organic and inorganic materials. The NMR spectrum of ^{113}Cd was recorded for only one resonance line owing to the spin $I = 1/2$. The ^{113}Cd NMR spectrum at 200 K is shown in the inset of Fig. 7. The ^{113}Cd NMR chemical shift was recorded using $CdCl_2O_8 \cdot 6H_2O$ as a standard. The ^{113}Cd NMR chemical shifts decreased as the temperature increased, and then increased slightly near T_C. Above T_C, the chemical shifts moved downfield, indicating that the surrounding environment of ^{113}Cd changed slightly near T_C.

The saturation recovery traces for the ^{113}Cd spectrum of the $N(CH_3)_4CdBr_3$ single crystal were measured using a static NMR

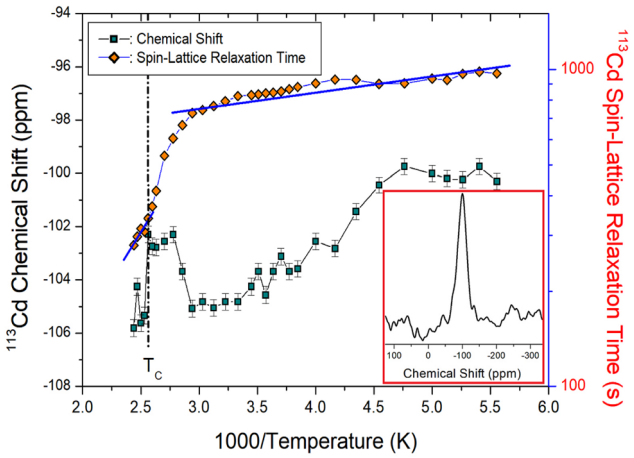

Fig. 7 Static NMR chemical shifts and spin–lattice relaxation times in the laboratory system T_1 for ^{113}Cd in $N(CH_3)_4CdBr_3$ single crystal as a function of inverse temperature. The slopes of the solid lines are represented activation energies ((Inset): The ^{113}Cd NMR spectrum at 200 K).

method; the recovery traces were satisfactorily fitted to a single-exponential function:[30]

$$P(\infty) - P(\tau)/P(\infty) = A\exp(-\tau/T_1) \quad (4)$$

where $P(\tau)$ is the nuclear magnetization at time τ. The recovery traces for the resonance line of the ^{113}Cd nuclei were measured by changing the delay times, and the ^{113}Cd T_1 values in the laboratory frame were obtained from the slope of the intensity *versus* delay time plot using eqn (4). The T_1 values are represented as functions of the inverse temperature in Fig. 7. Although the slope of the T_1 plot near T_C was roughly continuous, T_1 gradually decreased as the temperature increased, and then decreased rapidly above 340 K; T_1 at 300 K was as long as 825 s, and that at 410 K was shortened to 280 s. At all temperatures measured herein, the ^{113}Cd T_1 values were in the slow-motion range, where $\omega_C\tau_C \gg 1$, ${T_1}^{-1} \propto {\omega_C}^{-2}\exp(-E_a/k_BT)$.

The experimental value of T_1 was expressed in terms of the correlation time τ_C for the molecular motions based on the BPP theory:[35,37]

$$1/T_1 = R\{\tau_C/[1 + {\omega_C}^2{\tau_C}^2] + 4\tau_C/[1 + 4{\omega_C}^2{\tau_C}^2]\} = A\exp(-E_a/k_BT) \quad (5)$$

where R is a constant and ω_C is the Larmor frequency of Cd. The T_1 of ^{113}Cd for thermally activated reorientation follows the usual Arrhenius expression in eqn (5). The E_a values were determined from the slope of the semi-log plot of T_1 *vs.* 1000/temperature, represented by the orange squares in Fig. 7. The activation energies below and above 340 K were determined to be 1.23 ± 0.10 kJ mol^{-1} and 11.32 ± 2.57 kJ mol^{-1}, respectively.

4. Conclusion

The data confirm that $N(CH_3)_4CdBr_3$ crystallizes with a hexagonal structure having a phase transition temperature of 390 K. The NMR chemical shifts, linewidths, $T_{1\rho}$, and T_1 of the perovskite-type $N(CH_3)_4CdBr_3$ crystal were considered, aiming to understand the structural geometry and changes in the molecular dynamics during the high-temperature transition from phase I to II. Analysis of the ^{1}H, ^{13}C, and ^{14}N NMR chemical shifts of the cation with temperature showed that the surrounding structural geometry underwent a continuous change, without anomalous changes around T_C. However, the ^{113}Cd NMR chemical shifts showed a small change near T_C. $N(CH_3)_4CdBr_3$ crystal has a hexagonal structure both above and below the phase transition temperature, and only the space group is different. In relation to this, although the structural geometry changes around ^{1}H, ^{13}C, and ^{14}N were not significantly detected, the ^{113}Cd NMR chemical shifts are changed slightly near T_C. It is inferred that it is related to the arrangement of Cd in $CdBr_3$ groups. The linewidths of the ^{1}H, ^{13}C, and ^{14}N peaks of phase I were narrower than those of phase II, indicating that the motional averaging effects were caused by the rapid rotation of the $N(CH_3)_4$ group in phase I, resulting from the motional narrowing caused by the rapid rotation of the $N(CH_3)_4$ groups.

The $T_{1\rho}$ values for the ^{1}H and ^{13}C nuclei, and the T_1 values for ^{113}Cd were obtained with increasing temperature. The sudden changes in T_1 and $T_{1\rho}$ near T_C indicate a sudden variation in the energy transfer in the area surrounding the protons, carbons, and cadmium. The E_a obtained from the temperature-dependence of T_1 and $T_{1\rho}$ for ^{1}H, ^{13}C, and ^{113}Cd was generally ~1.2 kJ mol^{-1} below T_C and almost 14.5 kJ mol^{-1} above T_C, for phases I and II, respectively, where the E_a for phase I is ~12 times larger than that for phase II. Because the E_a of CH_3 is lower than that of $N(CH_3)_4$, the methyl group moves more easily and freely. The small values of E_a for phase II indicate a large degree of freedom for the methyl group and $CdBr_6$ octahedra in $N(CH_3)_4CdBr_3$. For phase I, the large values of E_a were primarily attributed to the overall molecular motion of $N(CH_3)_4$ and ^{113}Cd in the $CdBr_6$ groups. These results are supported by the following: the ^{113}Cd T_1 obtained herein changes rapidly near T_C, and the ^{79}Br NQR spectrum reported by other groups[25] also changes rapidly near T_C. Consequently, the phase-transition mechanisms of $N(CH_3)_4CdBr_3$ at high temperature are related to the reorientation of the $N(CH_3)_4$ group and arrangement of ^{113}Cd in the octahedral $CdBr_6$ groups. The results of this study on organic–inorganic hybrid perovskite-type $N(CH_3)_4CdBr_3$ are expected to facilitate their potential applications in various electrochemical devices such as supercapacitors, batteries, and fuel cells. In the future, this study may be able to provide a complete link between the structure, dynamics and NMR properties observed here by combining *Ab initio* molecular dynamics NMR calculations.[48,49]

Author contributions

A. R. Lim performed crystal growth, X-ray experiments, and wrote the manuscript. S. H. Kim measured NMR experiments.

Conflicts of interest

There are no conflicts to declare.

Acknowledgements

This work was supported by the National Research Foundation of Korea (NRF) grant funded by the Korean Government (MSIT) (2023R1A2C2006333) and the Basic Science Research Program through the NRF, funded by the Ministry of Education, Science, and Technology (2016R1A6A1A03012069).

References

1 I. Ruiz-Larrea, J. Diaz-Hernandez, A. Fraile-Rodriguez, A. Arnaiz, E. H. B. Canegra and A. Lopez-Echarri, *J. Phys.: Condens. Matter*, 1999, **11**, 2259.
2 T. Asahi and K. Izutsu, *J. Phys. Soc. Jpn.*, 2003, **72**, 330.
3 A. El-Korashy and M. G. Brik, *Solid State Commun.*, 2005, **135**, 298.
4 D. G. Sannikov, *Phys. Solid State*, 2005, **47**, 324.
5 F. Hlel, A. Ben Rhaeim and K. Guidara, *Russ. J. Inorg. Chem.*, 2008, **53**, 785.
6 S. Tancharakon, F. P. A. Fabbiani, D. R. Allan, K. V. Kamenev and N. Robertson, *J. Am. Chem. Soc.*, 2006, **128**, 9205.
7 J. S. Kim, M. Lee and A. R. Lim, *J. Appl. Phys.*, 2018, **124**, 205501.
8 S. Gonzalez-Carrero, R. E. Galian and J. Perez-Prieto, *Part. Syst. Char.*, 2015, **32**, 709.
9 W. Liu, J. Xing, J. Zhao, X. Wen, K. Wang, P. Lu and Q. Xiong, *Adv. Opt. Mater.*, 2017, **5**, 1601045.
10 I. Saikumar, S. Ahmad, J. J. Baumberg and G. Vijaya Prakash, *Scr. Mater.*, 2012, **67**, 834.
11 P. Mondal, S. K. Abdel-Aal, D. Das and S. K. Manirul Islam, *Catal. Lett.*, 2017, **147**, 2332.
12 M. Yuan, L. N. Quan, R. Comin, G. Walters, R. Sabatini, O. Voznyy, S. Hoogland, Y. Zhao, E. M. Beauregard, P. Kanjanaboos, Z. Lu, D. H. Kim and E. H. Sargent, *Nat. Nanotechnol.*, 2016, **11**, 872.
13 C. N. R. Rao, A. K. Cheetham and A. Thirumurugan, *J. Phys. Condens. Matter.*, 2008, **20**, 83202.
14 J.-P. Correa-Baena, M. Saliba, T. Buonassisi, M. Gratzel, A. Abate, W. Tress and A. Hagfeldt, *Science*, 2017, **358**, 739.
15 E. Edri, S. Kirmayer, M. Kulbak, G. Hodes and D. Cahen, *J. Phys. Chem. Lett.*, 2014, **5**, 429.
16 C. Eames, J. M. Frost, P. R. F. Barnes, B. C. O'Regan, A. Walsh and M. S. Islam, *Nat. Commun.*, 2015, **6**, 7497.
17 D. P. McMeekin, G. Sadoughi, W. Rehman, G. E. Eperson, M. Saliba, M. T. Horantner, A. Haghighirad, N. Sakai, L. Korte, B. Rech, M. B. Johnston, L. M. Herz and H. J. Snaith, *Science*, 2016, **351**, 151.
18 K. Venu, V. S. S. Sastry and J. Ramakrishna, *J. Phys. C: Solid State Phys.*, 1987, **20**, 1519.
19 P. Vanek, M. Havrankova, F. Smutny and B. Brezina, *Ferroelectrics*, 1990, **109**, 51.
20 T. Asahi, K. Hasebe and K. Gesi, *Acta Crystallogr., Sect. C: Cryst. Struct. Commun.*, 1990, **46**, 2252.
21 K. Gesi, *J. Phys. Soc. Jpn.*, 1990, **59**, 432.
22 M. N. Braud, M. Couzi and N. B. Chanh, *J. Phys.: Condens. Matter*, 1990, **2**, 8243.
23 M. N. Braud, M. Couzi, N. B. Chanh, C. Courseille, B. Gallois, C. Hauw and A. Meresse, *J. Phys.: Condens. Matter*, 1990, **2**, 8209.
24 T. Asahi, K. Hasebe and K. Gesi, *Acta Crystallogr., Sect. C: Cryst. Struct. Commun.*, 1991, **47**, 1208.
25 D. F. Baisa, E. D. Chesnokov, Z. V. Czapla, S. V. Pogrebnyak and I. G. Vertegel, *Acta Phys. Pol., A*, 1993, **84**, 271.
26 G. Aguirre-Zamalloa, G. Madariaga, M. Couzi and T. Breczewski, *Acta Crystallogr., Sect. B: Struct. Sci.*, 1993, **49**, 691.
27 D. F. Baisa, E. D. Chesnokov and Z. Czapla, *Acta Phys. Pol., A*, 1994, **86**, 357.
28 J. M. Igartua, G. Aguirre-Zamalloa, I. Ruiz-Larrea, M. Couzi, A. Lopez-Echarri and T. Breczewski, *J. Therm. Anal. Calorim.*, 1994, **41**, 1211.
29 Z. Czapla and S. Dacko, *Ferroelectrics*, 1996, **185**, 49.
30 A. R. Lim, *Appl. Magn. Reson.*, 2017, **48**, 297.
31 *SHELLXTL v6.10*, Bruker AXS, Inc., Madison, Wisconsin, USA, 2000.
32 A. R. Lim, *Sci. Rep.*, 2023, **13**, 6133.
33 A. Abragam, *The Principles of Nuclear Magnetism*, Oxford University Press, 1961.
34 C. Na and A. R. Lim, *Sci. Rep.*, 2023, **13**, 21008.
35 N. Bloembergen, E. M. Purcell and R. V. Pound, *Phys. Rev.*, 1948, **73**, 679.
36 J. L. Koenig, *Spectroscopy of Polymers*, Elsevier, 1999.
37 R. K. Harris, *Nuclear Magnetic Resonance Spectroscopy*, Pitman Pub., UK, 1983.
38 S. Albert, H. S. Gutowsky and J. A. Ripmeester, *J. Chem. Phys.*, 1972, **56**, 3672.
39 T. Tsuneyoshi, N. Nakamura and H. Chihara, *J. Magn. Reson.*, 1977, **27**, 191.
40 S. Sato, R. Ikeda and D. Nakamura, *Bull. Chem. Soc. Jpn.*, 1986, **59**, 1981.
41 S. Sato, R. Ikeda and D. Nakamura, *Ber. Bunsen-Ges. Phys. Chem*, 1987, **91**, 122.
42 K. J. Mallikarjunaiah, K. Jugeshwar Singh, K. P. Ramesh and R. Damle, *Magn. Reson. Chem.*, 2008, **46**, 110.
43 K. Pogorzelec-Glaser, J. Kaszyńska, A. Rachocki, J. Tritt-Goc, N. Piślewski and A. Pietraszko, *J. Chem.*, 2009, **33**, 1894.
44 P. A. Beckmann, C. E. Moore and A. L. Rheingold, *Phys. Chem. Chem. Phys.*, 2016, **18**, 1720.
45 B. V. S. Murthy, K. P. Ramesh and J. Ramakrishna, *Z. Naturforsch.*, 1993, **48a**, 868.
46 X. Guan and R. E. Stark, *Solid State Nucl. Magn. Reson.*, 2010, **38**, 74.
47 M. Y. Choi, S. J. Lee, H. Ju and A. R. Lim, *RSC Adv.*, 2022, **12**, 20679.
48 L. Szeleszczuk, D. M. Pisklak, M. Z. Pisklak and J. Com, *Chemistry*, 2019, **40**, 811.
49 A. H. Mazurek, L. Szeleszuk and D. M. Pisklak, *Int. J. Mol. Sci.*, 2021, **22**, 4378.